Journal of Mechanical Engineering and Automation 2015, 5(3A): 26-32
DOI: 10.5923/c.jmea.201501.05

Entropy Analysis of Combined Heat and Mass Transfer over a Plate Embedded in a Porous Medium

Meisam Habibi Matin

Department of Mechanical Engineering, Kermanshah University of Technology, Kermanshah, Iran

Abstract In this paper the second law analysis for heat and mass transfer over a plate embedded in a porous medium is conducted numerically. The governing continuity, momentum, energy and concentration equations are reduced to ordinary differential equations using similarity transformations. These equations are subsequently solved using an implicit finite difference scheme known as Keller-box method. The numerical data for velocity, temperature and concentration fields are used to compute local entropy generation, total entropy generation and Bejan number. The effects of Reynolds number, Schmidt number, Prandtl number, mass diffusion parameter, and concentration difference parameter on local entropy generation, total entropy generation, and Bejan number are reported.

Keywords Porous medium, Heat transfer, Mass transfer, Entropy generation

1. Introduction

Convective heat transfer over a plate embedded in a porous medium has many applications such as in petroleum production, separation processes in chemical engineering, thermal insulation systems, buildings, and nuclear reactors. In a pioneering paper, Cheng and Minkowycz [1] studied natural convection over a vertical plate with variable surface temperature with the plate embedded in a porous medium. Bejan and Poulikakos [2] investigated free convective boundary layer in a porous medium for non-Darcian regime. The mixed convective flow boundary layer over a vertical plate in porous medium was analysed by Merkin [3]. Kim and Vafai [4] studied the natural convective flow over a vertical plate embedded in porous medium. Chamkha [5] investigated the free convective flow in porous medium with uniform porosity ratio due to solar radiation flux. The MHD mixed convective flow over a vertical porous plate in porous saturated medium and assuming non-Darcian model was studied by Takhar and Beg [6]. Ranganathan and Viskanta [7] investigated the fluid mixed convective boundary layer over a vertical plate embedded in porous medium. They claimed that the viscous effects are significant and cannot be neglected. Kayhani et al. [8] studied the natural convection boundary layer along impermeable inclined surfaces embedded in a porous medium. Chamkha et al. [9] presented a non-similarity solution for natural convective flow over an inclined plate in porous medium due to solar radiation. Forced convection over a vertical plate in a porous medium was studied by Murthy et al. [10] with a non-Darcian model. They showed that the increase of solar radiation flux and also suction causes increase in Nusselt number and heat transfer rate. Kayhani et al. [11] studied local thermal non-equilibrium in porous media due to sudden temperature change and heat generation.

The use of second law of thermodynamics to analyze heat and fluid flow in engineering devices and systems has become increasingly important. This approach is driven by the realization among the thermal science community that the systems must be designed and operated so that the degradation of energy or the generation of entropy is minimized. There are various sources for entropy generation in engineering systems. In thermal systems, the main sources of entropy generation are heat transfer, mass transfer, viscous dissipation, electrical conduction, chemical reaction and coupling between heat and mass transfer as discussed by Bejan and co-workers in a series of pioneering publications [12-15]. The study of entropy generation in a liquid film falling along an inclined plate was performed by Saouli and Aïboud -Saouli [16]. Mahmud et al. [17] studied the case of mixed convection in a channel considering the effect of a magnetic field on the entropy generation. Aziz [18] investigated the entropy generation in a plane Couette flow for different boundary conditions at the plates. The effects of magnetic field and viscous dissipation on entropy generation in a falling liquid film were studied by Aïboud -Saouli et al. [19, 20]. Aïboud -Saouli and Saouli [21] conducted entropy generation analysis for viscoelastic MHD flow over a stretching sheet. They showed that the magnetic parameter, Hartman, Reynolds and Prandtl numbers cause

* Corresponding author:
habibimeisam@yahoo.com (Meisam Habibi Matin)
Published online at http://journal.sapub.org/jmea

the local entropy generation to increase. Rezaiguia et al. [22] investigated the effects of Prandtl and Eckert numbers on the local entropy generation in a forced convection boundary layer flow. They observed that with an increase in Eckert number or a decrease in Prandtl number, the local entropy generation increases. The general formulation for the local entropy generation in an incompressible flow of Newtonian fluid had been given by Hirschfelder et al. [23]. The entropy generation for combined forced convection heat and mass transfer in a two dimensional channel was investigated by San et al. [24].

In the present study, the second law analysis for heat and mass transfer over a plate embedded in a porous medium is investigated numerically. To the best of our knowledge, this problem has remained unexplored. The governing continuity, momentum, energy and concentration equations are reduced to ordinary differential equations with similarity transformations. The resulting equations are solved using an implicit finite difference scheme known as the Keller-box method. The local entropy generation is calculated using the numerical derived data for the velocity, temperature and concentration fields in the entropy generation expression derived by Bejan [12]. The total entropy generation is evaluated by integrating the local entropy generation data over the flow domain.

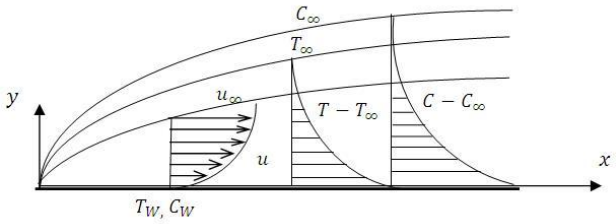

Figure 1. Schematic of flow model and coordinate system

2. Problem Formulation

Consider a stationary flat plate embedded in a porous medium of permeability *K* as illustrated in Fig.1. The continuity, momentum, energy and concentration equations for the two-dimensional boundary layer flow may be written as

$$\frac{\partial u}{\partial x}+\frac{\partial v}{\partial y}=0 \tag{1}$$

$$\rho\left(u\frac{\partial u}{\partial x}+v\frac{\partial u}{\partial y}\right)=\mu_{eff}\frac{\partial^2 u}{\partial y^2}-\frac{\mu_{eff}}{K}u \tag{2}$$

$$u\frac{\partial T}{\partial x}+v\frac{\partial T}{\partial y}=\alpha_{eff}\frac{\partial^2 T}{\partial y^2} \tag{3}$$

$$u\frac{\partial C}{\partial x}+v\frac{\partial C}{\partial y}=D_{eff}\frac{\partial^2 C}{\partial y^2} \tag{4}$$

subject to the following boundary conditions

$$\begin{aligned} &u=0, v=0, T=T_w, C=C_w \quad at \quad y=0\\ &u\to u_\infty, T\to T_\infty, C\to C_\infty \quad as \quad y\to\infty \end{aligned} \tag{5}$$

where the coordinate *x* is the distance along the plate, *y* is the coordinate normal to the plate, u and v are velocity components in *x* and *y* directions, respectively. The symbols T and C denote temperature and mass concentration at a general location (x, y) in the flow field, respectively. The plate is assumed to be a constant temperature T_w. The diffusing species at the plate have a fixed mass concentration C_w. The quantities T_∞ and C_∞ represent the ambient temperature and ambient mass concentration, respectively. Here, μ_{eff} is the effective dynamic viscosity of the fluid, ρ is the fluid density, α_{eff} is the effective thermal diffusivity of the medium, and D_{eff} is the effective mass diffusivity of the medium. The assumption that the effective viscosity is identical to dynamic viscosity is appropriate for packed beds of particles, and commonly used to describe boundary layer flows in a porous medium.

The following similarity variables are introduced to reduce the governing equations to ordinary differential equations:

$$\begin{aligned} &\psi=\left(\frac{u_\infty\mu_{eff}\ x}{\rho}\right)^{1/2} f(\eta),\ \theta(\eta)=\frac{T-T_\infty}{T_w-T_\infty},\\ &\phi(\eta)=\frac{C-C_\infty}{C_w-C_\infty},\ \eta=\frac{y}{x}\mathrm{Re}^{1/2} \end{aligned} \tag{6}$$

where the stream function $\psi(x,y)$ is defined as

$$u=\frac{\partial\psi}{\partial y},\quad v=-\frac{\partial\psi}{\partial x} \tag{7}$$

With the use of similarity variables, the continuity equation is automatically satisfied. The momentum equation (2), the energy equation (3), and the concentration equation (4) now appear as a set of coupled ordinary differential equations which may be written as

$$f'''+\frac{1}{2}ff''-\frac{1}{N_K}f'=0 \tag{8}$$

$$\theta''+\mathrm{Pr}\ f\theta'=0 \tag{9}$$

$$\phi''+Sc\ f\phi'=0 \tag{10}$$

where primes denote differentiation with respect to η. The boundary conditions take the following form:

$$\begin{aligned} &f(0)=0,\ \ f'(0)=0,\ \theta(0)=1,\ \phi(0)=1\\ &f'(\infty)=1,\ \theta(\infty)=0,\ \phi(\infty)=0 \end{aligned} \tag{11}$$

The dimensionless parameters *Sc*, *Re*, Pr, and N_K are Schmidt number, Reynolds number, Prandtl number, and permeability parameter, respectively, and defined as follows:

$$Sc=\frac{\mu_{eff}}{\rho D_{eff}},\ \mathrm{Re}=\frac{\rho u_\infty x}{\mu_{eff}},\ \mathrm{Pr}=\frac{\mu_{eff}\,C_P}{k},N_K=\frac{\rho u_\infty K}{x\,\mu_{eff}} \quad (12)$$

In view of the definitions of N_K and *Re*, a true similarity transformation is not achieved. Equations (8-11) must be interpreted as locally similar. The local similarity solution often provides a good preliminary insight into the problem.

3. Second Law Analysis

Using the boundary layer approximation, the entropy generation can be simplified as follows

$$S_G=\frac{k}{{T_\infty}^2}\left(\frac{\partial T}{\partial y}\right)^2+\frac{\mu}{T_\infty}\left(\frac{\partial u}{\partial y}\right)^2+\frac{\mu}{K\,T_\infty}u^2+ R\frac{D_{eff}}{C_\infty}\left(\frac{dC}{dy}\right)^2+R\frac{D_{eff}}{T_\infty}\left(\frac{dC}{dy}\right)\left(\frac{\partial T}{\partial y}\right) \quad (13)$$

wherein *R* is the gas constant.

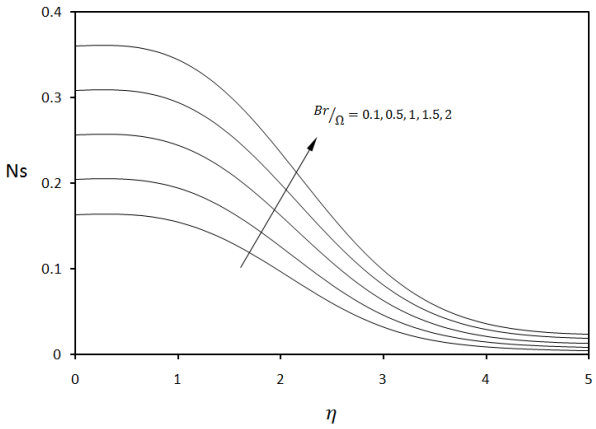

Figure 2. Local entropy generation for various values of dimensionless group parameter when $M_d=1,\lambda=0.05,\mathrm{Re}=1,\ N_K=10,\ \mathrm{Pr}=0.7,Sc=0.1$

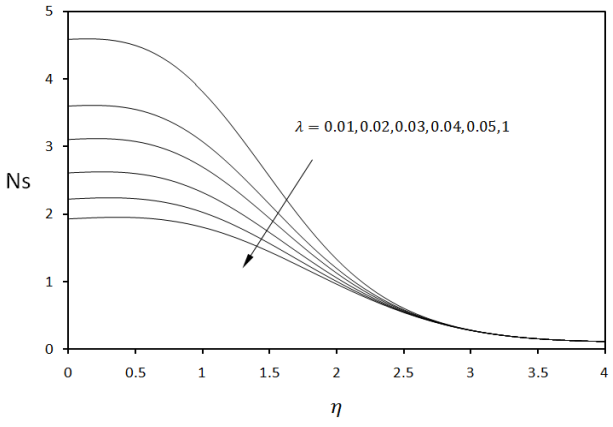

Figure 3. Local entropy generation for various values of dimensionless group parameter when $M_d=1,Sc=2,\ \mathrm{Re}=10,\ N_K=10,\ \mathrm{Pr}=0.7,Br/\Omega=0.1$

Using Eqs. (6) and (13), the entropy generation number is given by the following relationship in terms of the quantities appearing in Eqs. (8-10):

$$N_S=\mathrm{Re}\,\theta'^2+\mathrm{Re}\frac{Br}{\Omega}f''^2+\frac{Br\,\mathrm{Re}}{\Omega\,N_K}f'^2+\frac{M_d}{\lambda\ \Omega^2}\mathrm{Re}\,\phi'^2+\frac{M_d\ \mathrm{Re}}{\Omega}\phi'\theta' \quad (14)$$

Where

$$N_S=\frac{S_G}{(S_G)_0},(S_G)_0=\frac{k(\Delta T)^2}{{T_\infty}^2\,x^2} \quad (15)$$

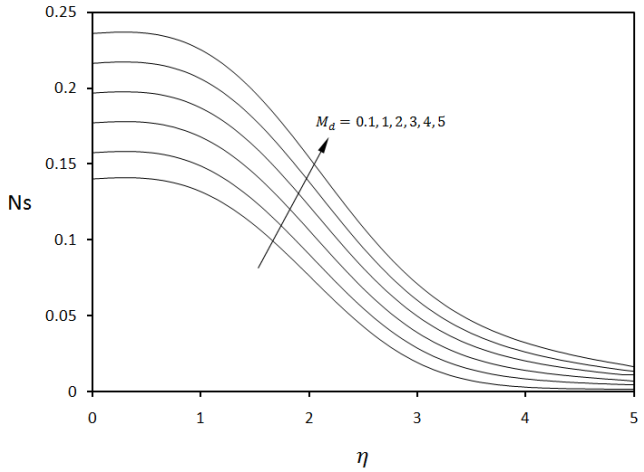

Figure 4. Local entropy generation for various values of Schmidt number $Sc=0.1,\lambda=0.05,\mathrm{Re}=1,N_K=10,\mathrm{Pr}=0.7,Br/\Omega=0.1$

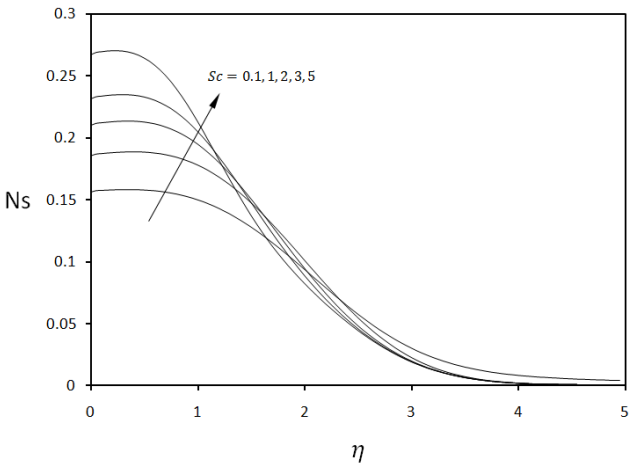

Figure 5. Local entropy generation for various values of Schmidt number when $M_d=1,\lambda=0.05,\mathrm{Re}=1,N_K=10,\mathrm{Pr}=3,Br/\Omega=0.01$

Re and *Br* are the Reynolds number and Brinkman number, respectively. Also Ω, λ M_d are the dimensionless temperature difference, the dimensionless concentration difference and the mass diffusion parameter, respectively. These three parameters are defined as follows:

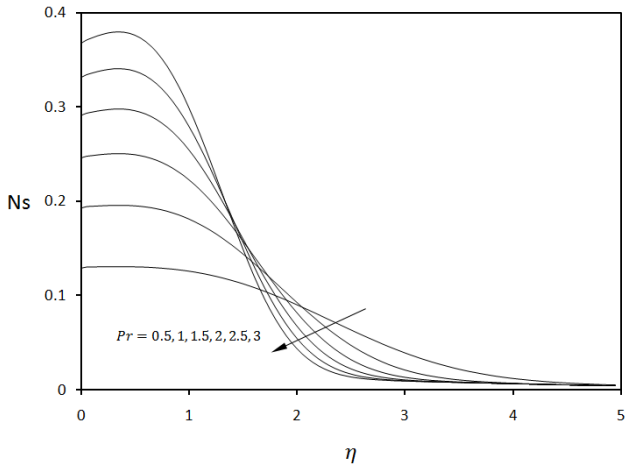

Figure 6. Local entropy generation for various values of Prandtl number when $M_d = 1, \lambda = 0.05, \mathrm{Re} = 1, N_K = 10, Sc = 0.1, Br/\Omega = 0.01$

$$\lambda = \frac{\Delta C}{C_\infty}, \Omega = \frac{\Delta T}{T_\infty}, Br = \frac{\mu_{eff}\, u_\infty{}^2}{k\Delta T},$$
$$M_d = \frac{R D_{eff}(\Delta C) T_\infty}{k\Delta T} \quad (16)$$

The total entropy generation, S, is evaluated by integrating of the local entropy generation over whole of the boundary layer domain as

$$S = \int_0^5 N_S d\eta \quad (17)$$

The choice of $\eta = 5$ was found to cover the three boundary layer regions in their entirety. Also, Bejan number was calculated as the ratio of the entropy generation due to heat transfer S_T to the total entropy generation S i.e.

$$Be = \frac{S_T}{S} \quad (18)$$

4. Numerical Procedure

Eqs. 8-11 are solved numerically using an efficient implicit finite-difference scheme known as Keller-box method. The method is implemented in four steps. First, Eqs. 8-10 are reduced to seven first-order differential equations. Second, the equations are discretized using central finite differences. Third, the resulting nonlinear algebraic equations are linearized using Newton's method [26-28] and written in matrix vector form. The fourth and final step uses the block-tridiagonal-elimination technique to solve the linearized algebraic equations. A step size of $\Delta\eta = 0.005$ was found to satisfy the convergence criterion of 0.001 in all cases. As noted earlier, the choice of $\eta = 5$ satisfactorily covered the three boundary layer regions in their entirety.

5. Results and Discussion

Numerical computations were performed to study the effects of various dimensionless parameters on the local entropy generation, the total entropy generation and Bejan number. Figure 2 shows the local entropy generation in boundary layer as function of dimensionless group Br/Ω which may be viewed as a measure of viscous dissipation in the flow. The curves in Fig.2 show that the increase in viscous dissipation leads to increase in local entropy generation. Because of large velocity gradients in the region near the plate, this near-plate region generates more entropy compared with that generated in the region far from the plate. As the concentration difference parameter λ is increased, the local entropy generation is reduced as can be seen in Fig.3. Figure 4 shows as the mass diffusion parameter M_d increases, the local entropy generation increases. Again, the region near the plate experiences larger entropy genera- tion compared with the region further into the flow field. Fig. 5 illustrates the sensitivity of local entropy generation to Schmidt number *Sc*. Although the effect of Schmidt number does not appear explicitly in the entropy generation equation (15), its influence on entropy generation is exerted through the velocity, temperature, and mass concentration characteristics which are governed by Eqs. (8-11) which contain *Sc*.

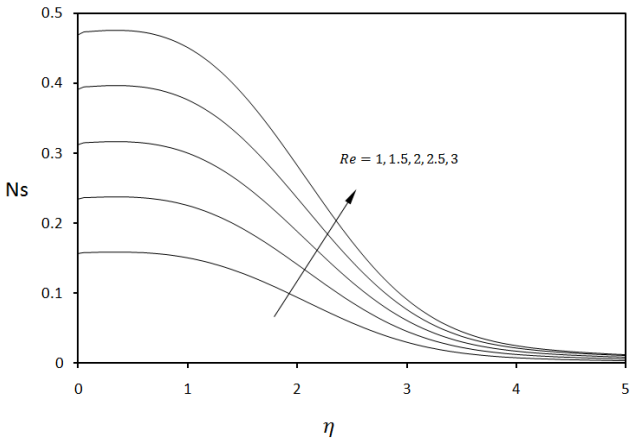

Figure 7. Local entropy generation for various values of Reynolds number when $M_d = 1, \lambda = 0.05, \mathrm{Pr} = 0.7, N_K = 10, Sc = 0.1, Br/\Omega = 0.01$

While in the region near the plate, the local entropy generation increases with *Sc*, it has an opposite effect in the region far from the plate, though the opposite effect is not that distinctly manifested. The effect of Prandtl number on the local entropy generation presented in Fig. 6 is similar to that of Schmidt number observed in Fig. 5. In the region closer to the plate, as Prandtl number increases, heat transfer from the plate increases which in turn leads to increased entropy generation. Figure 7 displays the local entropy generation as a function of Reynolds number, *Re*. The increase in local entropy generation due to increase in *Re* may be attributed to the increase in free stream velocity u_∞

which produces an increase in heat transfer and hence an increase in entropy generation. The effect of permeability parameter N_K on local entropy generation is illustrated in Fig.8. For the combination of variables chosen for preparing Fig.8, the local entropy generation decreases only slightly with the increase in the permeability of the medium.

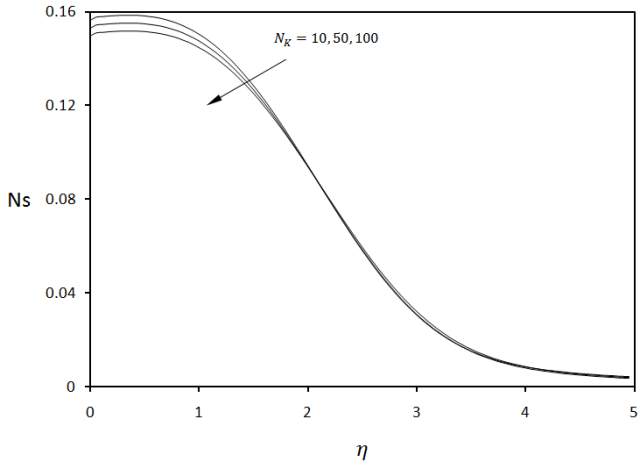

Figure 8. Local entropy generation for various values of permeability parameter N_K when $M_d = 1, \lambda = 0.05, \Pr = 0.7, \mathrm{Re} = 1, Sc = 0.1, Br/\Omega = 0.01$

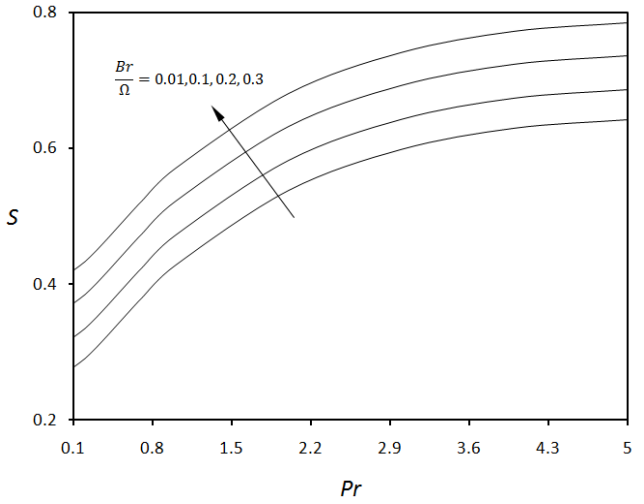

Figure 9. Total entropy generation versus Prandtl number for various values of dimensionless group parameter when $M_d = 1, \lambda = 0.05, N_K = 10, \mathrm{Re} = 1, Sc = 0.1$

Attention is now turned to the total entropy generated over the entire flow field. Figure 9 demonstrates that the total entropy generated increases significantly as *Pr* and *Br/Ω* increase. The increase in *Pr* enhances the heat transfer which in turn increases the entropy generation. However, the effect of *Pr* on entropy generation is subdued beyond *Pr* = 3. The increase in *Br/Ω* implies an increase in fluid friction irreversibility (increase in *Br*) or a decrease in dimensionless temperature ratio *Ω*. In both cases, the result is increased entropy generation. Figure 10 shows that the total entropy generation increases almost linearly with the mass diffusion parameter M_d for all four values of Schmidt number *Sc*. For a fixed M_d, the total entropy generated increases significantly as Schmidt number increases from 0.1 to 3.0 but further increase in Schmidt number appears to increase the total entropy generation only slightly. The functional dependence of total entropy generation on Reynolds number and dimensionless concentration difference is shown in Fig.11. The total entropy generation increases as Reynolds number (and hence the transfer) increases, but decreases slightly as the concentration potential driving the mass transfer i.e. - C_∞ (= λ C_∞) increases. In other words, a stronger mass transfer process tends to attenuate the total entropy generation slightly. Fig.12 shows that the total entropy generation increases as Prandtl number (and hence heat transfer) increases. However, the increase in permeability of the medium i.e. N_K tends to reduce entropy generation slightly.

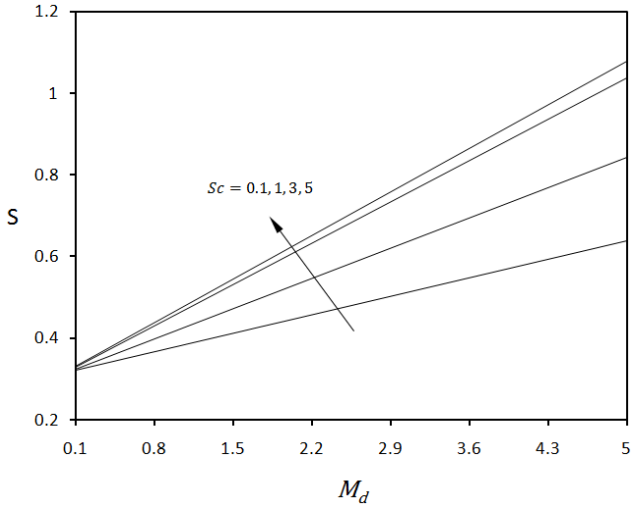

Figure 10. Total entropy generation versus mass diffusion parameter for various values of Schmidt number when $N_K = 1, \lambda = 0.05, \Pr = 0.7, \mathrm{Re} = 1, Br/\Omega = 0.01$

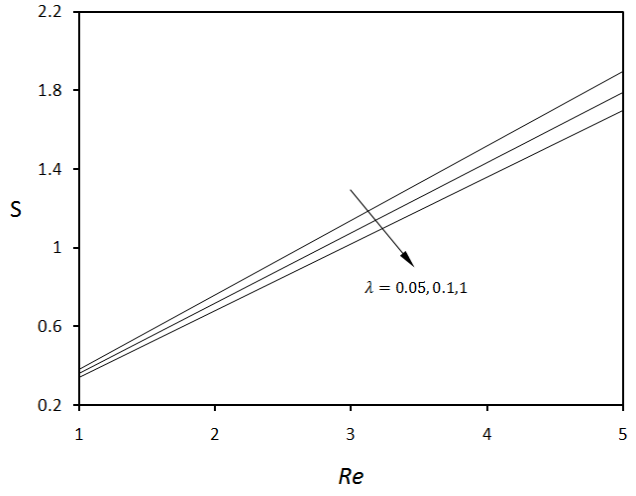

Figure 11. Total entropy generation versus Reynolds number for various values of dimensionless concentration difference when $M_d = 1, Br/\Omega = 0.01, Sc = 0.1, \Pr = 0.7, N_K = 10$

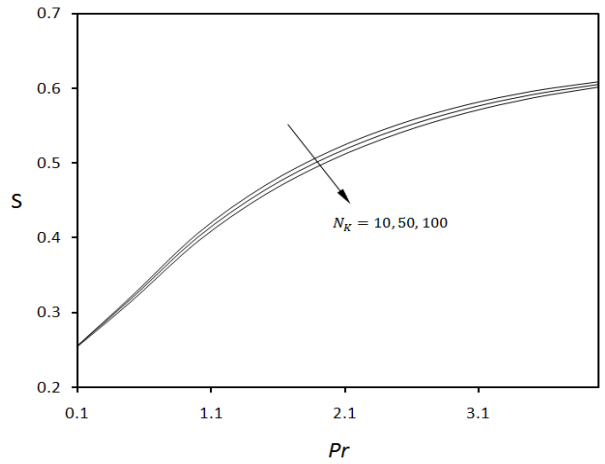

Figure 12. Total entropy generation versus Prandtl number for various values of permeability parameter when $M_d = 1, \lambda = 0.1, Sc = 0.1,$ $\mathrm{Re} = 1, Br/\Omega = 0.01$

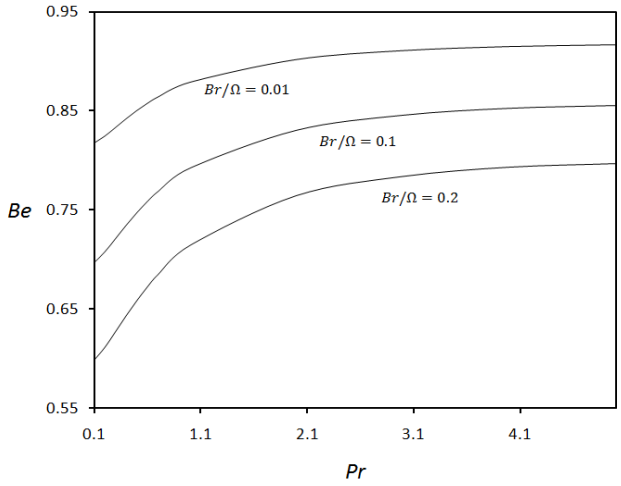

Figure 13. Bejan number versus Prandtl number for various values of dimensionless group parameter when $M_d = 1, \lambda = 0.1, Sc = 0.1,$ $\mathrm{Re} = 1, N_K = 10$

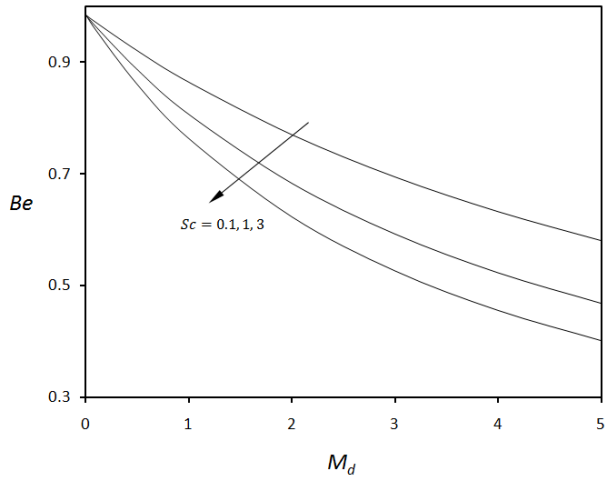

Figure 14. Bejan number versus mass diffusion parameter for various values of Schmidt number when $Br/\Omega = 0.01, \lambda = 0.1, \mathrm{Pr} = 0.7,$ $\mathrm{Re} = 1, N_K = 10$

The functional dependence of Bejan number on Prandtl number and dimensionless grouping Br/Ω illustrated in Fig.13 leads to two observations. First, for a fixed Br/Ω, the heat transfer irreversibility increases as Prandtl number increases, which in view of the definition (Eq.18), is reflected in higher Bejan number. Second, for a fixed Prandtl number, the entropy generation due to heat transfer S_T is fixed. Now, if Br/Ω is reduced, the total entropy generation S decreases because of a reduction in friction irreversibility. For fixed S_T, the reduction in S increases the Bejan number as suggested by Eq. 18. Fig.14 depicts Bejan number as a function of mass diffusion parameter M_d and Schmidt number Sc. Because the Prandtl and Reynolds numbers are fixed, the entropy generated due to heat transfer S_T is fixed. Thus any increase in M_d and/or Sc increases the total entropy generated S and consequently reduces Bejan number which is exactly what Fig.14 reveals. As M_d increases, the curves spread out, indicating that the effect of Sc on Bejan number is more pronounced. Figure 15 highlights the effect of concentration parameter λ and Reynolds number Re on Bejan number. The increase in Bejan number due to increase in Re is due to the increase in heat transfer irreversibility S_T. For fixed Re, Bejan number increases with λ because increase in λ reduces the total entropy generation S.

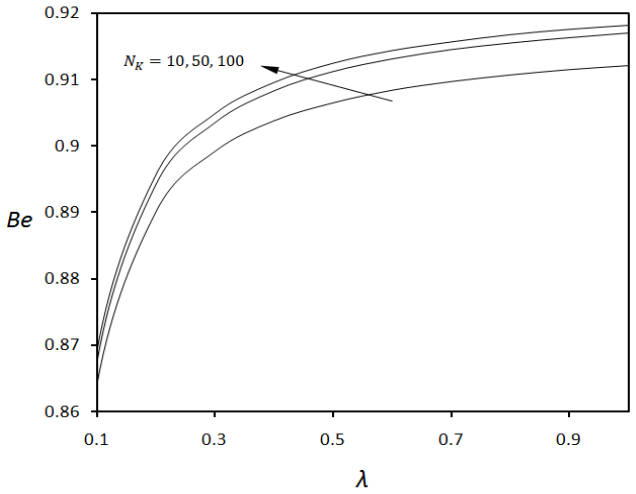

Figure 15. Bejan number versus dimensionless concentration difference for various values of permeability parameter when $M_d = 1,$ $Br/\Omega = 0.01,\ Sc = 0.1,\ \mathrm{Pr} = 0.7, \mathrm{Re} = 1$

REFERENCES

[1] P. Cheng, W. J. Minkowycz, Free convection about a vertical plate embedded in a porous medium with application to heat transfer from a dike, J. Geophys. 82 (1977) 2040-2044.

[2] A. Bejan, D. Poulikakos, The non–Darcy regime for vertical boundary layer natural convection in a porous medium, Int. J. Heat Mass Transfer 27 (1984) 717-722.

[3] J. H. Merkin, Mixed convection boundary layer flow on a

vertical surface in a saturated porous medium, Journal of Engineering Mathematics 14 (1980) 301-313.

[4] S. J. Kim, K. Vafai, Analysis of natural convection about a vertical plate embedded in a porous medium, Int. J. Heat Mass Transfer 32 (1989) 665-677.

[5] A. J. Chamkha, Solar radiation assisted natural convection in uniform porous medium supported by a vertical flat plate, J. Heat Transfer 119 (1997) 35-43.

[6] H. S. Takhar and O. A. Bèg, Effects of transverse magnetic field, Prandtl number and Reynolds number on non-Darcy mixed convective flow of an incompressible viscous fluid past a porous vertical flat plate in a saturated porous medium, Int. J. Energy Research 21 (1997)87-100.

[7] P. Ranganathan, R. Viskanta, Mixed convection boundary-layer flow along a vertical surface in a porous medium, Num. Heat Transfer 7 (1984) 305–317.

[8] M. H. Kayhani, E. A. O. Khaje, M. Sadi, Natural convection boundary layer along impermeable inclined surfaces embedded in porous medium, Mechanika 17 (2011) 64-70.

[9] A. J. Chamkha, C. Issa, K. Khanafer**,** Natural convection from an inclined plate embedded in a variable porosity porous medium due to solar radiation, Int. J. Therm. Sci. 41 (2002) 73-81.

[10] P. V. S. N. Murthy, S. Mukherjee, D. Srinivasacharya, P. V. S. S. S. R. Krishna, Combined radiation and mixed convection from a vertical wall with suction/injection in a non–Darcy porous medium, Acta Mechanica 168 (2004) 145–156.

[11] M. H. Kayhani, A. O. Abbasi, M. Sadi, Study of local thermal nonequilibrium in porous media due to temperature sudden change and heat generation, Mechanika 17 (2011) 57-63.

[12] A. Bejan, Second-law analysis in heat transfer and thermal design, Adv. Heat Transfer 15 (1982) 1–58.

[13] A. Bejan, Entropy Generation Minimization, CRC Press, Boca Raton, Florida, 1996.

[14] A. Bejan, A study of entropy generation in fundamental convective heat transfer, J. Heat Transfer 101 (1979) 718–725.

[15] A. Bejan, The thermodynamic design of heat and mass transfer processes and devices, Int J. Heat and Fluid Flow, 8 (1987) 259-276.

[16] S. Saouli, S. Aïboud-Saouli, Second law analysis of laminar falling liquid film along an inclined heated plate, Int. Comm. Heat Mass Transfer 3 (2004) 879–886.

[17] S. Mahmud, S. H. Tasnim, H. A. A. Mamun, Thermodynamic analysis of mixed convection in a channel with transverse hydromagnetic effect, In. J. Therm. Sci. 42 (2003) 731–740.

[18] A. Aziz, Entropy generation in pressure gradient assisted Couette flow with different thermal boundary conditions, *Entropy* 8 (2006) 50-62.

[19] S. Aïboud-Saouli, S. Saouli, N. Settou, N. Meza, Thermodynamic analysis of gravity-driven liquid film along an inclined heated plate with hydromagnetic and viscous dissipation effects, Entropy 8 (2006) 188–199.

[20] S. Aiboud-Saouli, N. Settou, S. Saouli, N. Meza, Second-law analysis of laminar fluid flow in a heated channel with hydro-magnetic and viscous dissipation effects, Appl. Energy 84 (2007) 279–289.

[21] S. Aïboud-Saouli, S. Saouli, Entropy analysis for viscoelastic magnetohydrodynamic flow over a stretching surface, International Journal of Non-Linear Mechanics 45 (2010) 482–489.

[22] I. Rezaiguia, K. Mahfoud, T. Kamel, N. Belghar, S. Saouli, Numerical simulation of the entropy generation in a fluid in forced convection on a plane surface while using the method of Runge-Kutta, European Journal of Scientific Research 42 (2010) 637-643.

[23] J. O. Hirschfelder, C. F. Curtiss, R. B. Bird, Molecular Theory of Gases and Liquids, John Wiley, New York, 1954.

[24] J. Y. San, W. M. Worek, Z. Lavan, Entropy generation in combined heat and mass transfer, Int. J. Heat Mass Transfer, 30 (1987) 1359-1369.

[25] L. C. Woods, Thermodynamics of Fluid Systems, Oxford University Press, Oxford, 1975.

[26] T. Cebeci, P. Bradshaw, Momentum Transfer in Boundary Layers, Hemisphere Publishing Corporation, New York, 1977.

[27] T. Cebeci , P. Bradshaw, Physical and Computational Aspects of Convective Heat Transfer, Springer-Verlag, New York, 1988.

[28] M. Z. Salleh, R. Nazar, S. Ahmad, Numerical solutions of the forced boundary layer flow at a forward stagnation point, European Journal of Scientific Research 19 (2008) 644 – 653.

[29] A. Bejan, Convection Heat Transfer. Wiley, New York, 1984, p. 31.